Geochemical processes influencing arsenic mobility at Bullendale historic gold mine, Otago, New Zealand

L Haffert [a] & D Craw [a]

[a] Geology Department , University of Otago , Dunedin, New Zealand
Published online: 27 Sep 2010.

PLEASE SCROLL DOWN FOR ARTICLE

Taylor & Francis
Taylor & Francis Group

Geochemical processes influencing arsenic mobility at Bullendale historic gold mine, Otago, New Zealand

L Haffert and D Craw*

Geology Department, University of Otago, Dunedin, New Zealand

The historic Bullendale gold mine processed arsenopyrite-rich ore from mesothermal deposits in the South Island of New Zealand from 1864 to 1907. No site rehabilitation was undertaken upon mine closure and processing waste contains arsenic concentration of up to 40 wt%. Originally, all of this arsenic was present as arsenopyrite and with time it has been replaced by secondary arsenic phases. Waste evolution has resulted in a mineralogical gradation of arsenic phases between the ferrihydrite with varying amounts of adsorbed arsenic, amorphous iron arsenates and crystalline kankite, scorodite and zykaite. The stability of the secondary arsenic phases is favoured at low pH (pH 3, <0.1 mg/L) and, at present, reactions associated with iron arsenate dissolution ensure a prevailing pH window of c. 2.5 to 3.5. However, an increase in pH through flooding could destabilise the secondary arsenic minerals resulting in a substantial increase of arsenic solubility (>100 mg/L). In addition to the battery site, an upstream adit is a continuous source of dissolved arsenic to the environment. Due to the alkaline pH conditions in catchment water, arsenic remains mobile and dissolved As of c. 0.03 mg/L is detectable in Skippers Creek more than 2km downstream. Even when this anomaly has been diluted, the arsenic flux of the river is still predominantly controlled by the adit input.

Keywords: arsenic mobility; secondary arsenic minerals; historic mine; process residue; mesothermal

Introduction

Arsenic (As) is a trace metalloid which is of increasing environmental concern because of its toxicity at relatively low (ppb) levels (e.g., Foy et al. 1978; Smedley & Kinniburgh 2002) and consequent risk to plants, animals, and human health. Arsenic is commonly associated with metallic mineral deposits, especially as arsenopyrite and arsenian pyrite in mesothermal gold deposits, where it can be naturally enriched up to levels of hundreds to thousands of times above the average crustal abundance (Hutchison & Ellison 1992; Craw 2001; Craw & Pacheco 2002). While arsenic is naturally mobilised from these deposits, mining and beneficiation of the deposits can significantly amplify arsenic mobilisation. Once the ore has been excavated, processed, and discarded in waste rock piles and tailing, percolating rainwater can facilitate oxidation and dissolution of arsenic from the mine wastes and mine excavations. Dissolved arsenic can then be discharged into the environment with potentially toxic consequences for the downstream biota (Foy et al. 1978; Smedley & Kinniburgh 2002).

New Zealand has a long history of gold mining and associated elevated arsenic concentrations are common, especially around historic gold mine sites in the South Island (Craw et al. 2000; Hewlett et al. 2005; Craw et al. 2007; Haffert & Craw 2008a). One of these sites is the historic Bullendale gold mine and its processing site, the Phoenix battery (Fig. 1) which operated from 1864 to 1907. Similar to other historic gold mines, arsenic-rich concentrates from the

processing were disposed of outside the battery plant or into the adjacent stream without environmental control and no rehabilitation was undertaken after mine closure. This paper identifies and characterises primary and secondary arsenic phases in the Bullendale mine waste. These phases are evaluated in the context of the environmental pH, which controls related dissolved arsenic mobility (Dove & Rimstidt 1985; Krause & Ettel 1988). Based on these observations, predictions of mineralogical evolution and associated arsenic mobility can be made. In addition, changes in arsenic mobility in response to anomalous events, such as naturally occurring flooding or overriding of prevailing pH through site remediation measures, are theoretically quantified. The overall impact of the Bullendale mine site on catchment water quality, especially with respect to natural background contribution, is then estimated based on total dissolved arsenic concentrations and arsenic flux.

General setting

Geology

The basement rocks of the studied area are part of the Otago Schist belt (Fig. 1), which is c. 150 km wide. The protolith rocks are of Permian–Triassic age and are composed of orogenic calc-alkaline andesitic to granodioritic sediments that originally accumulated on the Gondwana margin (MacKinnon 1983). Moderate-pressure regional metamorphism during the late Jurassic deformed and recrystallised the

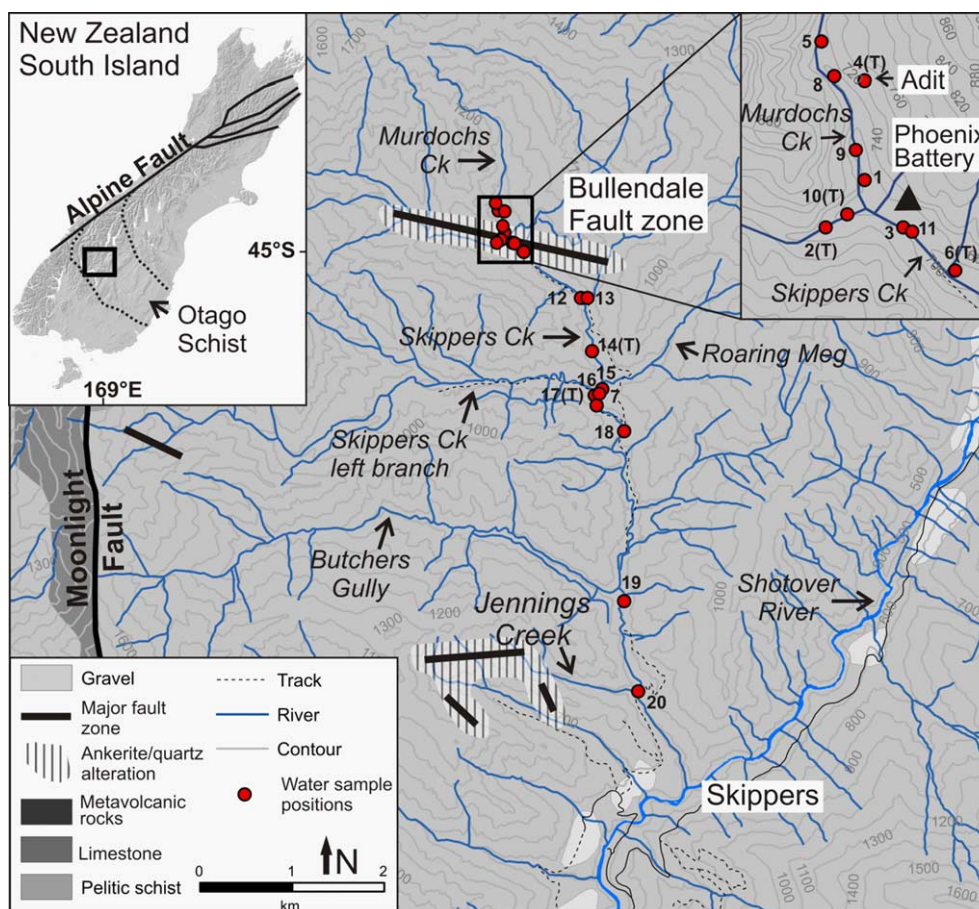*Corresponding author. Email: dave.craw@stonebow.otago.ac.nz

Fig. 1 Topographic map of the Skippers Creek catchment. Bullendale fault zone and other major fault zones are drawn after Begbie & Craw (2006), Craw et al. (2006), and MacKenzie et al. (2007) and alteration halos (hatched) are added after Craw et al. (2006). Major rock types are also shown (grey shades). Rivers and sites discussed in the text are annotated and water samples positions and their labels are added. The inset digital elevation model of the South Island of New Zealand shows the extent of the Otago Schist and the location of Skippers Creek catchment.

sediments to quartzofeldspathic greywacke and argillite. The metamorphic grade of the Otago Schist belt is dominated by greenschist facies, especially in the central part of the belt (Mortimer 1993, 2000). The studied area is dominated by pelitic schist, with only minor metavolcanic rocks (Fig. 1). The pre-mineralisation greenschist facies have an assemblage of quartz, albite, muscovite, chlorite and calcite, with accessory epidote and titanite (Craw 2002). Minor mafic metavolcanics also occur. Cenozoic sediments, also affected by several phases of deformation, originally covered most of the basement rocks. Because of erosion only local areas are now covered by the Cenozoic sediments.

During the metamorphic and uplift history of the basement schist, gold (Au) bearing quartz veins were emplaced as a result of long-continued hydrothermal fluid flow associated with the underlying tectonic processes (Craw 1989; Craw & Norris 1991). The Bullendale gold deposits are part of a swarm of mineralised fault zones (Fig. 1) that formed during the development of the Moonlight Fault in the middle Tertiary (Cooper et al. 1987; Craw et al.

2006). These intensely altered faults are characterised by abundant quartz and subordinate albite veins, silicified breccias and wall rocks. Sulfides, especially arsenopyrite and to a lesser extent stibnite, and gold (MacKenzie et al. 2007) are also commonly associated with the faults. Gold can be enriched up to 45 g/t (mg/kg) (Williams 1974), whereas arsenic levels can reach up to 10,000 mg/kg (MacKenzie et al. 2007). Apart from some localised stibnite occurrences, antimony (Sb) concentrations are only weakly elevated with concentration up to 14 mg/kg and are likely to occur in solid solution or micro-inclusions in the arsenopyrite (MacKenzie et al. 2007). Major mineralised faults can have an alteration halo of hydrothermally altered rocks extending up to 150 m across strike. These are dominated by direct replacement of metamorphic chlorite by ankerite or ferroan dolomite (MacKenzie et al. 2007) (Fig. 1). However, despite the widespread ankerite and dolomite formation in altered rock, magnesium concentrations (typically 1–2 wt%) do not differ significantly from unaltered rocks (MacKenzie et al. 2007).

Catchment and site description

The studied area is located in a mountainous, semi-arid region in a subhumid climatic zone (Rosen & Jones 1998). Average temperature minima in Queenstown (30 km south of the studied area) are 10°C in summer and 0.1°C in winter, with average temperature maxima of 22°C and 10°C, respectively. The general area receives < 600 mm of annual precipitation (Rosen & Jones 1998), an order of magnitude less than the coastal areas to the west. Potential evaporation always exceeds precipitation, except in winter. The vegetative cover is dominated by tussock and scattered shrubs.

The Bullendale mining area is drained by Skippers Creek and one of its small tributaries, Murdochs Creek (Fig. 1). Skippers Creek has numerous small- and medium-sized tributaries downstream of the site, of which the most notable are the Roaring Meg, Skippers Creek Left Branch, and Butchers Gully (Fig. 1). Skippers Creek was studied over a length of c. 7 km, of which the upper 350 m are part of Murdochs Creek (Fig. 1).

Skippers Creek flow rate is c. 1000 L/s at the lower end of the catchment, at which point it drains a catchment of c. 80 km^2. The Skippers Creek catchment drains steep mountainous country (Fig. 1) with the highest peak being Mt Aurum (2245 m) at the northwest border of the catchment. Intense erosion, especially mechanical associated with the steep terrain, inhibits *in situ* chemical weathering, and natural outcrops in the Bullendale area are exceptionally fresh (Craw et al. 2006). Because of the fast erosion rate only a thin soil cover developed, and on steep slopes soil is absent. Accordingly, river sediment in Skippers Creek catchment contains mainly freshly eroded sediment, including pyrite, and is largely devoid of clay minerals. The extent of hydrothermal ankerite formation associated with the Bullendale fault zone is clearly visible as thin orange iron oxyhydroxide or ferrihydrite staining on clasts and outcrops in the riverbed. Substantial ferrihydrite precipitates are, however, absent from Skippers Creek sediment. Scattered boulders of mineralised rocks can also be found throughout the catchment and many of these contain fresh sulphide minerals exposed on their surfaces.
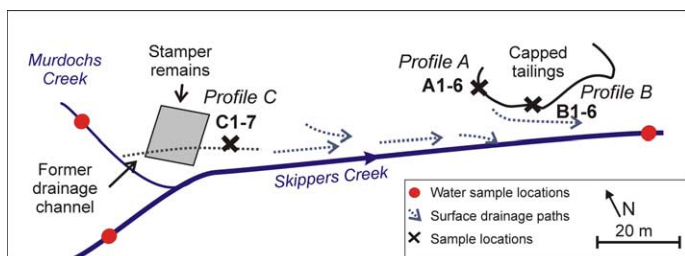

Fig. 2 Schematic site outline of the Phoenix battery site showing the principal water flow directions and sampling positions for water. Locations of mine waste sampling Profiles A, B, and C are indicated.

The Phoenix battery site, located at the confluence of Murdochs Creek and Skippers Creek, is of historic value and still includes the foundations of the burnt-out 30-stamp Phoenix battery (Fig. 2). Processing waste can be found adjacent to the battery foundations and in a spoil heap at the downstream end of the site (Fig. 2). Most of the site drainage enters Skippers Creek just after the confluence with Murdochs Creek. An adit is located c. 350 m upstream of the battery site, directly adjacent to Murdochs Creek (Fig. 1) and the adit continuously discharges water into the creek. The battery site has been severely disturbed by periodic flooding of Murdochs Creek in a drainage channel that passes closer to the site than the currently active streambed (Fig. 2).

Methods

Sampling

Two sampling campaigns took place. The first (Nov 2006) focused on site geochemistry and was targeted at materials that were suspected to have been affected by ore processing activities. These include the spoil heap at the downstream end of the site, which has a defined edge where it has been eroded away by the river. Samples were taken at 10 locations along two profiles (Profile A and B, Fig. 2, Fig. 3) through the river-eroded scarp. Six samples (100 g each) of different materials were taken from a 1.5 m exposed profile of the substrate by the stamper foundations, in the bank of a former drainage channel (Profile C, Fig. 2, Fig. 3).

The paste pH of c. 10 g solid materials was determined in the field from slurries made with distilled water in a clean plastic container using the method of Sobek et al. (1978). In addition, preliminary water samples were taken during this first campaign, including adit discharge water that enters Murdochs Creek 350 m upstream of the battery site. About 200 g of ferrihydrite precipitate at the adit entrance was extracted as a wet slurry and sealed in a clean plastic bag.

The second sampling campaign (Mar 2007) focused on downstream arsenic chemistry and the impact of mineralised rocks and their processing at the Phoenix battery. Thirteen water samples were taken over a distance of c. 7.5 km with increasing intervals away from the site (Fig. 1). A 1 L sample was taken for major ions and a 100 ml sample was taken for arsenic analyses at each locations. At 12 of the water sample locations, sediment samples from depositional areas favouring small grain size were also extracted. For dissolved arsenic analysis, all water samples were filtered in the field (0.45 μm) and collected in nitric acid-washed plastic bottles, in which the sample was acidified to a pH of 2 with nitric acid. Simultaneously, a second unfiltered sample was collected for major ion analysis. Water sampling was accompanied by *in situ* pH measurement with an Oakton PC10 field pH meter.

Estimates of flow rates for small seeps and creeks were made by timing the collection of water flow in a container of

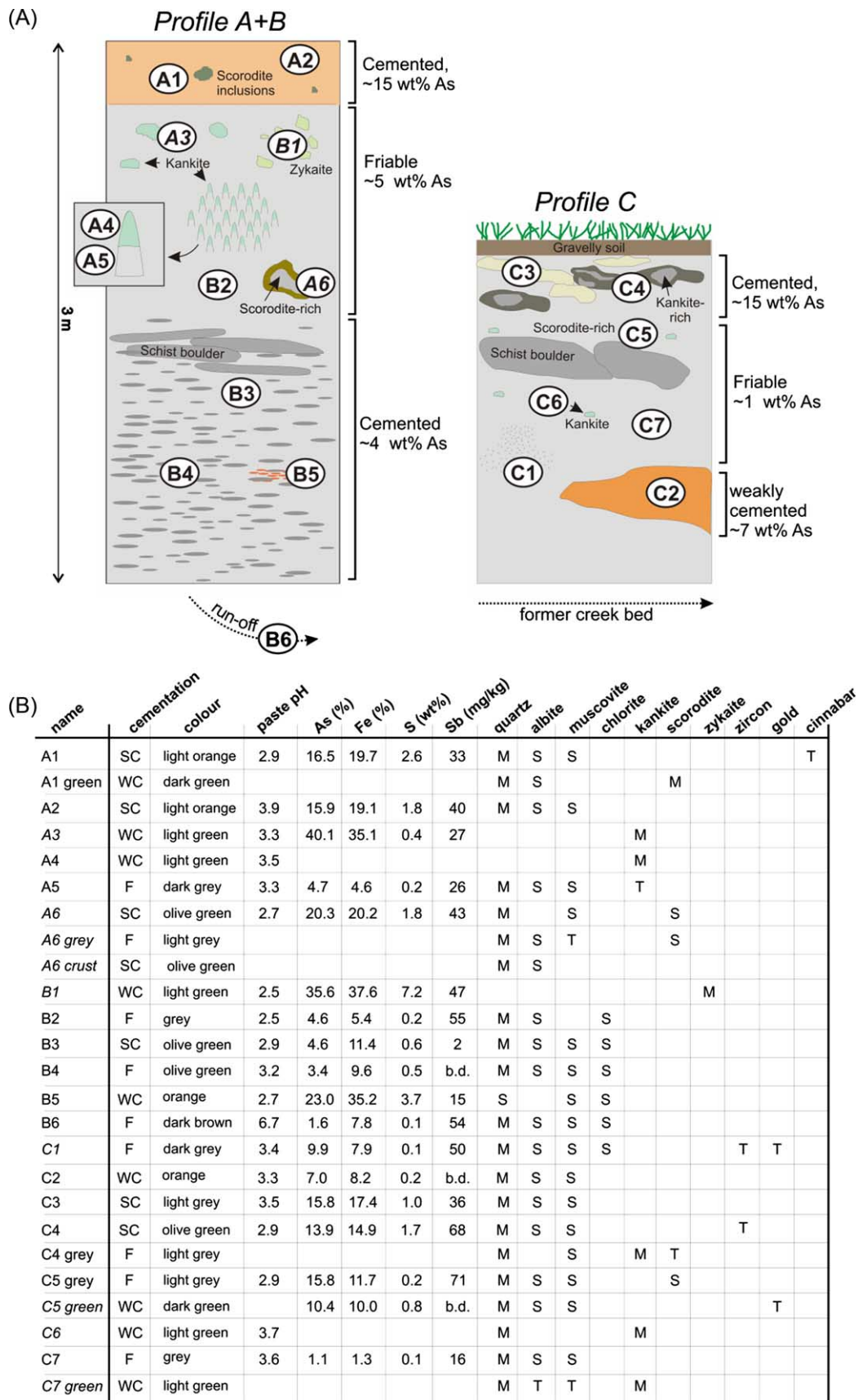| name	cementation	colour	paste pH	As (%)	Fe (%)	S (wt%)	Sb (mg/kg)	quartz	albite	muscovite	chlorite	kankite	scorodite	zykaite	zircon	gold	cinnabar
A1	SC	light orange	2.9	16.5	19.7	2.6	33	M	S	S							T
A1 green	WC	dark green						M	S			M					
A2	SC	light orange	3.9	15.9	19.1	1.8	40	M	S	S							
A3	WC	light green	3.3	40.1	35.1	0.4	27					M					
A4	WC	light green	3.5									M					
A5	F	dark grey	3.3	4.7	4.6	0.2	26	M	S	S		T					
A6	SC	olive green	2.7	20.3	20.2	1.8	43	M		S			S				
A6 grey	F	light grey						M	S	T			S				
A6 crust	SC	olive green						M	S								
B1	WC	light green	2.5	35.6	37.6	7.2	47							M			
B2	F	grey	2.5	4.6	5.4	0.2	55	M	S		S						
B3	SC	olive green	2.9	4.6	11.4	0.6	2	M	S	S	S						
B4	F	olive green	3.2	3.4	9.6	0.5	b.d.	M	S	S	S						
B5	WC	orange	2.7	23.0	35.2	3.7	15	S		S	S						
B6	F	dark brown	6.7	1.6	7.8	0.1	54	M	S	S	S						
C1	F	dark grey	3.4	9.9	7.9	0.1	50	M	S	S	S				T	T	
C2	WC	orange	3.3	7.0	8.2	0.2	b.d.	M	S	S							
C3	SC	light grey	3.5	15.8	17.4	1.0	36	M	S	S							
C4	SC	olive green	2.9	13.9	14.9	1.7	68	M	S	S					T		
C4 grey	F	light grey						M		S		M	T				
C5 grey	F	light grey	2.9	15.8	11.7	0.2	71	M	S	S			S				
C5 green	WC	dark green		10.4	10.0	0.8	b.d.	M	S	S						T	
C6	WC	light green	3.7					M				M					
C7	F	grey	3.6	1.1	1.3	0.1	16	M	S	S							
C7 green	WC	light green						M	T	T		M					

Fig. 3 (A) Sampling details in Profiles A, B and C (Fig. 2). Italic sample labels indicate that the material was not necessarily *in situ*. (B) Analytical results (based on XRF), including As, Fe and S concentrations, and mineralogy (based on XRD and EDS methods). Minerals are classified as present in major (M), subordinate (S) and trace (T) amounts. The degree of cementation is indicated with strongly cemented 'SC', weakly cemented 'WC', and friable 'F'. The abbreviation 'b.d.' indicates that the analyte was below the detection limit.

known volume over a known period of time. For larger streams and rivers, a floating object was timed over a known distance of near-constant cross-sectional area. Although crude, these methods provide better than order-of-magnitude estimates of flow rates (Hewlett et al. 2005).

Analytical methods

Water samples were analysed for dissolved As (detection limit 'd.l.' 0.001 mg/L) and Sb (d.l. 0.002 mg/L) by inductively-coupled plasma mass spectrometry (ICP-MS) at Hill Laboratories, Hamilton, New Zealand—an internationally accredited laboratory. Methods comply with standard methods for the examination of water and waste water (American Public Health Association [APHA] 2005). These include a four-point standard calibration curve (0.005, 0.010, 0.025, 0.050 mg/L), filter blanks and bottle blanks, and a synthetic control reference standard per run. All blanks and standards are made with ultra pure, trace metal-free water. At least one duplicate sample is run every 20 samples. Interference of $^{40}Ar^{35}Cl$ on ^{74}As analysis was corrected by measuring ^{77}Se and ^{82}Se and establishing the interference of $^{40}Ar^{37}Cl$ on ^{77}Se. This was then related to the $^{40}Ar^{35}C$ interference by adjusting for the natural abundance of both Cl isotopes.

Hill Laboratories also determined the anion/cation profile, including the following tests: pH, electrical conductivity (EC; d.l. 0.1 mS/m), alkalinity (d.l. 1 mg/L as $CaCO_3$), bicarbonate (d.l. 1 mg/L at 25°C), dissolved calcium (d.l. 0.05 mg/L), dissolved magnesium (d.l. 0.02 mg/L), dissolved sodium (d.l. 0.02 mg/L), dissolved potassium (d.l. 0.05 mg/L), chloride (d.l. 0.5 mg/L), sulfate (d.l. 0.5 mg/L).

All solid samples were oven-dried at 45°C for at least 48 hours. Stream sediment samples were subsequently sieved to $< 64 \mu m$, thus excluding coarse quartz-rich material. Mine processing residues, including the ferrihydrite sample from the mine entrance, were manually ground into powder in an agate mortar and pestle. Clean pulverised quartz was ground between samples to minimise cross-contamination. Sediment samples were then analysed for total recoverable As and Sb by nitric/hydrochloric acid digestion (EPA 200.2; United States Environmental Protection Agency [US-EPA] 1994) followed by solution analysis by ICP-MS (Hill Laboratories, Hamilton, New Zealand). Interference of $^{40}Ar^{35}Cl$ on ^{74}As analysis was corrected as described above. Trace element analyses were performed on pressed powder disks prepared from 5 g of ground sample bound with 5 mL of Moviol binding solution. Because of the unusually high concentrations of arsenic involved, internal laboratory standards (arsenopyrite-bearing quartz) were used in addition to international standards at low As concentrations. X-ray fluorescence spectrometer (XRF) analyses were performed at the Geology Department of the University of Otago, New Zealand, with a Philips PW2400 XRF equipped with a PW 2510 Sample Changer. Owing to the exceptionally high As and Fe

concentrations in the samples, the Kβ line was used instead of the stronger Kα line for these elements.

Mineral constituents were identified by X-ray diffraction (XRD) on powder discs or, if the sample volume did not allow for pressed powdered discs, on glass slides. In the case of millimetre to centimetre scale heterogeneous samples, a powdered disc of the composite sample was prepared, while glass slides were prepared of an alcohol-based slurry of individual sub-samples of the composite sample. The analysis was conducted with a PANalytical X'Pert-Pro MPD PW3040/60 also at the Geology Department of the University of Otago. The scanning was conducted with Cu Kα radiation at a rate of 0.05 °/s. Results were interpreted with the support of the PANalytical High Score software package.

Polished thin sections of 10 variably cemented tailings samples were produced. Friable samples were soaked in glue before processing. The thin sections were examined with a semi-automated JEOL JXA-8600 electron microprobe analyser (EPMA) at the University of Otago, New Zealand. Electron backscatter imaging (BSE) as well as scanning electron microscopy (SEM) was applied. Individual mineral compositions were obtained by qualitative energy dispersive analysis (EDS). Counting times for EDS was 100 s and the microprobe was operated using a beam current of 2.00×10^{-9} mA and an accelerating voltage of 15.0 kV. EDS was not calibrated for total concentrations and was only used to determine relative concentrations.

Results

Description of processing waste

The Phoenix battery site is characterised by an abundance of very arsenic-rich mine waste (1–40 wt% As). Much of this arsenic-rich waste is intimately admixed with orange-brown ferrihydrite, which is largely X-ray amorphous 2-line ferrihydrite. The waste material exposed in Profile A and B (Fig. 2, Fig. 3) is dominated by fine- to medium-sized subangular quartz grains with micrometre-scale, angular, interstitial material of quartz albite and muscovite. Traces of cinnabar and gold were also found (c. 50 μm). In the absence of secondary precipitation, porosity can be as high as 30%. The material is strongly heterogeneous and within the Profile A and B three distinct horizons can be identified (Fig. 3): (1) an upper (top 10–30 cm) light-orange, strongly cemented crust, capping the underlying material. Arsenic and Fe are relatively high is this horizon (16 and 20 wt%, respectively) and the paste pH ranges between 3.0 and 3.5; (2) an unconsolidated, grey, middle horizon that is characterised by rare to abundant schist clasts and cemented fragments (cm-scale). Arsenic concentrations are significantly lower than in the overlying crust (c. 5 wt%) and paste pH can be as low as 2.5; (3) the lower horizon hosts abundant schist clasts (cm-scale) and these are often aligned. Arsenic concentrations are

slightly lower in this horizon (c. 4 wt%) and the paste pH averages c. 3.

Material exposed at Profile C can also be divided into three different horizons (Fig. 3): (1) an upper crust, which is similar in character to the crust found at Profile A and B; (2) the main body of sediment, which is made up of well-sorted sand-sized homogenous quartz dominated sediment with little or no interstitial detrital material and/or coating of clasts. This material contains some of the lowest arsenic concentrations encountered at this site (1 wt%); (3) a discontinuous orange horizon of weakly to strongly cemented sediment embedded within the main body of sediment. The material is similar in character to the surrounding homogeneous sediment, with the exception of an orange precipitate cementing the sediment. Arsenic concentrations are also higher in this horizon (7–8 wt%).

Secondary arsenic phases

Arsenic within the Phoenix battery waste piles can occur as a variety of phases (Fig. 4), including: (a) scorodite, a common hydrated iron arsenate ($FeAsO_4 \cdot 2H_2O$); (b) kankite, which is essentially further-hydrated scorodite ($FeAsO_4 \cdot 3.5H_2O$); (c) zykaite, which is an iron arsenate that also incorporates sulfur ($Fe_4(AsO_4)_3(SO_4)(OH) \cdot 15H_2O$); and (d) amorphous iron arsenate, arsenical ferrihydrite (Paktunc et al. 2008), and ferrihydrite with adsorbed arsenate. The absence of arsenolite (As_2O_3) from this list is not certain. If traces of arsenolite are present, its major peaks may have been masked in the diffractograms by albite, which is common at this site (Fig. 3). Arsenolite typically occurs in mine wastes where ore has been roasted (Haffert & Craw 2008a), and roasting was not

mentioned in any of the Phoenix battery historic accounts (Hamel 2001; Petchey 2002, 2006).

The dominant arsenic phase at the Phoenix battery site is largely amorphous iron arsenate that pervades the processing residues. Crystalline arsenic phases, such as scorodite, kankite, and zykaite, are locally concentrated and are generally less common (Fig. 3). From the pure kankite sample (sample A3, Fig. 3), a standard spectrum for the EDS was generated. Most of the amorphous As-rich Fe phases inspected under the microprobe have similar As/Fe peak ratios to this kankite spectrum. Stoichiometric As/Fe ratios based on bulk sample composition plot close to crystalline iron arsenates in the As-Fe-S ternary diagram (Fig. 4), suggesting that the majority of the amorphous As-rich iron phase are likely to be amorphous iron arsenates. Some precipitates have higher Fe peaks and lower As peaks than the kankite EDS spectrum, and these are presumed to be dominated by ferrihydrite, with some As incorporated (Fig. 4). This material is probably at least partly arsenical ferrihydrite.

The arsenic-rich phases have a wide range of textures and morphologies (Fig. 5). Crystalline arsenic minerals can occur as discreet centimetre scale globular aggregations displaying acicular growth (Fig. 5A, B). Mainly kankite, and to a lesser extent zykaite occur in this form. The amorphous ferric arsenate and Fe-rich precipitates typically act as interstitial cements (Fig. 5C). The upper layer of the waste piles, the crust, is especially well cemented, with little or no porosity. Some of the As-rich Fe phases occur as interstitial micrometre scale grains (Fig. 5D). These can form either as globular growth, as individual scattered spherules or as angular fragments. The individual spherules are likely to be the precursor to the globular growth, which itself can be a precursor to the cement. Similar morphology has already been observed in the scorodite cement described by Haffert & Craw (2008a), where it was also suggested that the globular growth is a precursor to the cement. The angular fragments are likely to be derived from fragmentation of that cement during erosion. The amorphous As-rich Fe phases can also occur as coatings on grains in the silicate waste, causing red-brown staining (Fig. 5E). Coating of grains is most pronounced within the orange horizon of Profile C (Fig. 5E). Here, all of the quartz grains were covered in a thin orange precipitate, which was very evident due to high porosity and absence of interstitial grains (Fig. 5E).

In rare instances, a secondary As-rich Fe phase was found to replace arsenopyrite grains, which resulted in prismatic internal structure, and locally contained trace amounts of sulfur (Fig. 5F). Original pyrite and arsenopyrite were not identified at this site. It is likely that this replacement process was once a common occurrence within the waste piles, but with the decomposition of pyrite and the continuous evolution of the secondary arsenic minerals, evidence of this replacement has become rare.
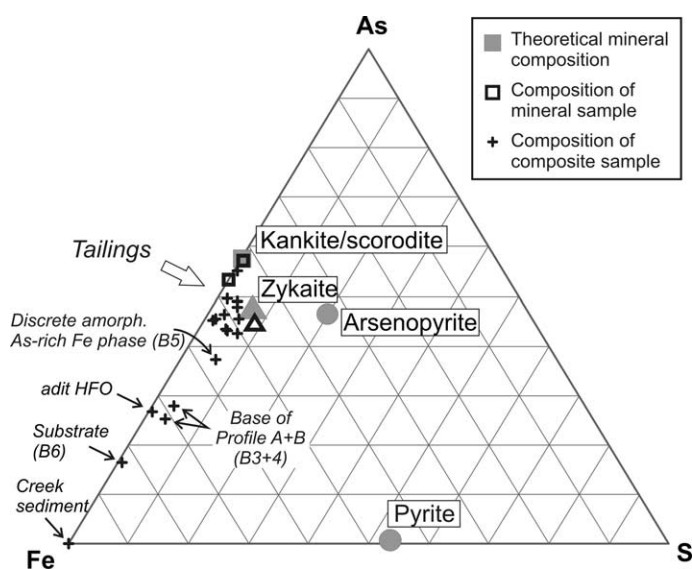

Fig. 4 Ternary diagram based on wt% of As-Fe-S. Samples of discrete mineral phases are indicated as hollow symbols. The composition of kankite/scorodite, zykaite, arsenopyrite, and pyrite are added for comparison (full symbols).
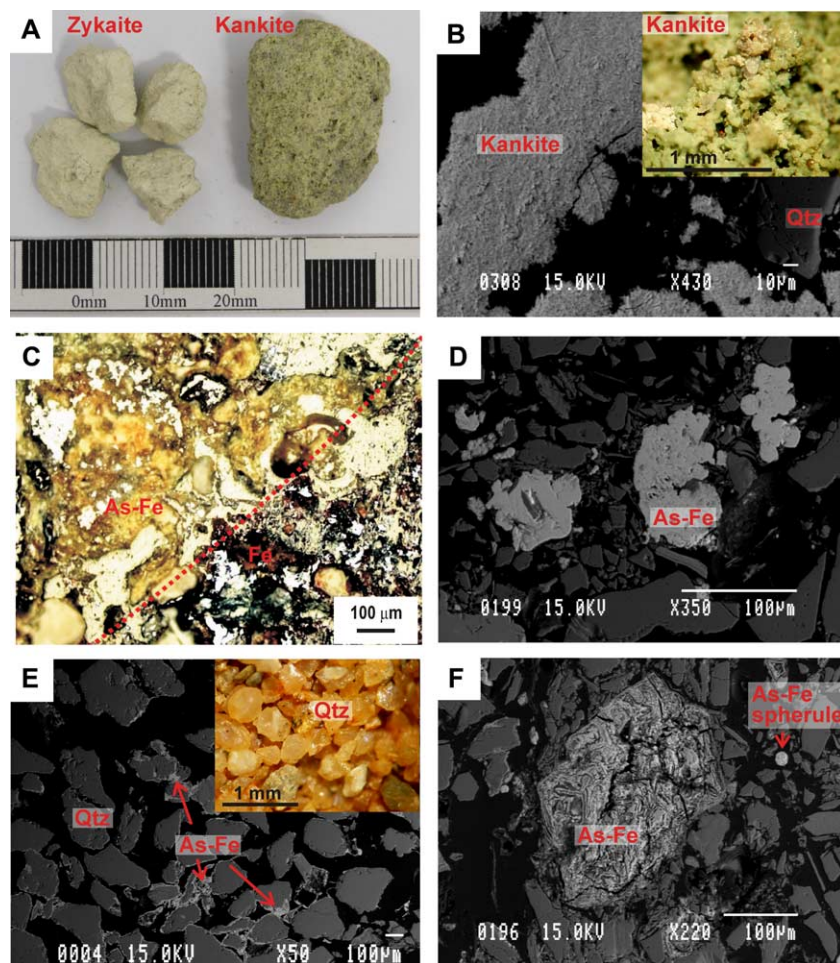
Fig. 5 Arsenic phases and their morphology. (**A**) Photograph of discrete centimetre-scale globular aggregations of zykaite (sample B1) and kankite (sample A3). (**B**) Backscatter electron (BSE) image of a kankite aggregate with an inset of a microscopic photograph of kankite (sample A3). (**C**) Reflected light microscopic image (plane polarised light) of a cemented portion of sample A6. Upper left half is cemented with pale green iron arsenate (As-Fe), and lower right is cemented with brown ferrihydrite (Fe) containing minor As. Boundary between two cement types is dashed. (**D**) BSE image of interstitial globular growth of As-rich Fe phases (sample C1). (**E**) BSE image of As-rich ferrihydrite coatings on quartz with an inset of microscopic photograph showing the typical orange colour of this As-bearing phase (sample C2). (**F**) BSE image of an arsenopyrite grain pseudomorphically replaced by iron arsenate (sample C1).

Water composition

Major ions

Regional background water and Skippers Creek catchment water are characterised by high bicarbonate concentrations and, with the exception of the adit water, all samples belong to the group of calcium bicarbonate waters (Fig. 6). The adit water, which has interacted with exposed mineralised host rock, is calcium magnesium bicarbonate sulfate water (Fig. 6). No detectable chloride (d.l. 0.5 mg/L) was encountered in any of the samples. The pH of all these waters is alkaline, with most ranging from 8.0 to 8.5. The adit water has a pH of 7.1 (Table 1). Samples taken from the same position during the preliminary and second sampling campaigns showed that all major ion concentrations were c. 30% lower during the preliminary campaign in spring (Table 1).

The composition of the surface waters passing the Phoenix battery are affected by several tributaries (Fig. 1 and Fig. 7). The adit discharge water enters Murdochs Creek c. 350 m upstream of the battery site, and then Murdochs Creek enters the three times larger Skippers Creek at the Phoenix battery site. Several tributaries enter Skippers Creek downstream of the battery site. These water mixing stages directly affect the observed compositions of the waters. The adit discharge water contains 3 to 4 times more bicarbonate, calcium, and sulfate and over an order of magnitude more magnesium than the background water (Fig. 7, Table 1). This elevated magnesium decreases when diluted by Skippers Creek. Over the following 7 km, major ion concentrations are only noticeably modified by the discharge of the two largest tributaries and the general trend of the hydrochemical facies with distance from the battery site is towards the calcium bicarbonate endmember (Fig. 6).
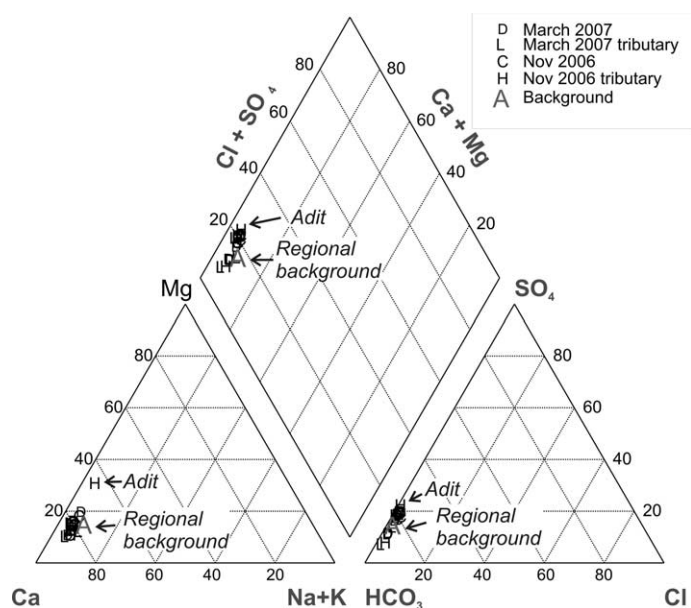
Fig. 6 Piper diagram of surface water collected in Skippers Creek catchment upstream and downstream of the Phoenix battery (Table 1 and Fig. 1).

Dissolved and sediment arsenic

Arsenic concentrations were generally 30–50% lower during the preliminary sampling campaign than in the later campaign (Fig. 7). Background levels in both Murdochs Creek and Skippers Creek approached are close to analytical detection limit (0.001–0.004 mg/L). The adit discharge water contained 0.54 mg/L As during the first sampling campaign and this raised Murdochs Creek arsenic concentrations to anomalously high levels (0.058 and 0.11 mg/L, Fig. 7). The elevated arsenic from Murdochs Creek and from the Phoenix battery site are considerably diluted downstream of the confluence (0.013 and 0.026 mg/L). Downstream of the battery, dissolved arsenic in Skippers Creek mirrors the trend observed for most major ions (Fig. 7). Concentrations remain unchanged, unless diluted by the major tributaries, which carry background arsenic concentrations. At 7 km downstream of the site, dissolved arsenic levels persist near 0.006 mg/L (Fig. 7).

The localised ferrihydrite precipitate at the adit entrance contains 16 wt% As. The precipitate forms a metre-scale apron at the adit entrance, but the apron does not reach Murdochs Creek. Sediment arsenic concentrations range between 17 mg/kg upstream from the adit and 65 mg/kg (Fig. 8) immediately downstream of the adit. The slightly anomalous sediment arsenic concentrations in Murdochs Creek are lowered close to background values by Skippers Creek sediment, which contains 24 mg/kg As. Arsenic in sediment drops steadily to 25 mg/kg until input from arsenic-rich sediment (61 kg/mg) from Butchers Gully at 2.5 km downstream of the site, and this increases arsenic in Skippers Creek sediment to 30 mg/kg. Subsequently, arsenic

concentrations continue near 30 mg/kg to 7 km downstream of the site (Fig. 8).

In contrast to the strong arsenic signal, antimony (Sb) concentrations in sediment and dissolved in the river water rarely exceed the detection limit of the analysis (Table 1). This is in accordance with strong As enrichment (up to 10,000 mg/kg) and the comparatively weak Sb enrichment during mineralisation (< 14 mg/kg) with only trace stibnite at this site.

Arsenic mobility in processing residues

The ultimate source of most arsenic in the mine waste was primary arsenopyrite in the ore concentrates. Even if arsenopyrite itself is not present in detectable amounts in the waste any more, its pseudomorphs, composed of secondary arsenic phases, can still be found at this site (Fig. 5F). Natural oxidation of arsenopyrite typically results in release of arsenate oxyanions to the surficial environment, accompanied by acidification (Fig. 9A; Haffert & Craw 2008a, b). Some of this dissolved arsenic enters the hydrosphere, but a significant amount is immobilised by incorporation into arsenical ferrihydrite (Paktunc et al. 2008), or is adsorbed to ferrihydrite precipitates (Roddick-Lanzilotta et al. 2002; Craw et al. 2004). Up to 16 wt% As was adsorbed onto fresh ferrihydrite precipitate at the adit entrance upstream of the Phoenix battery.

Despite the absence of pyrite and arsenopyrite in the waste, which are common sources of acidification upon weathering, all samples from the Phoenix battery mine waste fall into a pH window between pH 2.5 and 3.5. Here, acidification of circum-neutral water occurs from the dissolution of iron arsenate, producing ferrihydrite, arsenate, and one proton (Reaction 1, Fig. 10). Once the pH drops to about 3 (depending on Fe concentrations, Fig. 10), iron arsenate dissolution produces $FeOH^{2+}$ rather than $Fe(OH)_3$, and one proton is consumed rather than produced (reaction 2, Fig. 10). If Fe concentrations exceed 10^{-2} mol/L, this process ceases to take place. In that case, the lower pH limit is entirely controlled by the stability boundary between the $H_2AsO_4^-$ and H_3AsO_4 arsenate species at a pH of 2.2. At this boundary, iron arsenate dissolution does not further acidify the system (Reaction 3A, Fig. 10) and the onset of the conversion of $H_2AsO_4^-$ to H_3AsO_4 consumes protons, thereby counteracting further acidification (Reaction 3B, Fig. 10). Consequently, the initial acidification through iron arsenate dissolution can not acidify the system to a pH lower than 2.2, creating a pH window in the Phoenix battery waste from about 2.5 to 3.5, with the lower limit being independent of the amount of iron arsenate present in the material.

Arsenic mobility in the mine waste is closely linked to the solubilities of iron arsenates. These are generally not well known thermodynamically, with the exception of scorodite, and scorodite commonly behaves in a disequilibrium manner in natural situations (Krause & Ettel 1988; Dove & Rimstidt

Table 1 Major ion data including dissolved and sediment concentrations of As and Sb

Sample	pH	T °C	Cl mg/L	SO4$^-$ mg/L	Alkalinity (bicarbonate) mg/L	Ca mg/L	Mg mg/L	Na mg/L	K mg/L	Charge balance %	Dissolved As mg/L	Dissolved Sb mg/L	As in sediment mg/kg	Sb in sediment mg/kg
Regional background	6.6	10	2.0	14.1	107	33.7	3.8	3.9	1.4					
1	8.4	8	<1.0	12.2	63	19.2	2.7	1.17	0.66	−1.0	0.058	<0.0002		
2$_T$	8.5	9	<1.0	14.2	77	24.0	2.7	1.00	0.74	−2.3	0.003	<0.0002		
3	8.6	9	<1.0	13.8	75	23.4	2.7	1.03	0.72	−1.9	0.013	<0.0002		
4$_T$	7.1	8	<1.0	42.2	188	48.2	13.7	2.90	1.25	−2.9	0.536	0.0007	160000	
5	8.3	8	<1.0	7.9	45	14.3	1.1	0.86	0.53	−2.2	0.001	<0.0002		
6$_T$	8.5	9	<1.0	3.6	54	15.5	1.2	0.98	0.58	−1.1	0.001	0.0007		
7	8.5	9	<1.0	9.6	59	18.0	1.9	1.09	0.60	−1.6	0.007	<0.0002		
8	8.1	9	<1.0	12.8	66	22.4	1.7	1.2	0.66	−0.8	0.004	<0.0005	17	<0.4
9	8.2	9	<1.0	19.8	101	30.0	4.7	1.9	0.83	−2.0	0.11	<0.0005	65	<0.4
10$_T$	8.4	11	<1.0	19.5	110	35.3	4.0	1.5	0.96	−0.6	0.004	<0.0005	24	<0.4
11	8.3	11	<1.0	19.7	108	33.6	4.1	1.7	0.94	−1.6	0.026	<0.0005	28	<0.4
12	8.4	11	<1.0	19.6	107	33.7	4.1	1.6	0.93	−1.1	0.027	<0.0005	29	<0.4
13	8.4	14	<1.0	19.0	106	33.3	4.0	1.6	0.91	−1.2	0.024	<0.0005	30	<0.4
14$_T$	8.1	13	<1.0	6.7	52	15.3	1.4	1.6	0.56	−1.5	0.002	<0.0005		
15	8.4	15	<1.0	13.8	83	26.6	2.9	1.6	0.77	0.2	0.015	<0.0005	25	<0.4
16	8.3	15	<1.0	12.6	82	24.8	2.8	1.7	0.73	−1.4	0.013	<0.0005	26	<0.4
17$_T$	8.21	12	<1.0	4.3	71	20.9	1.5	1.1	0.59	−1.0	0.002	0.0014	61	0.6
18	8.23	14	<1.0	7.3	75	22.5	2.0	1.4	0.65	−0.6	0.006	0.0009	30	<0.4
19	8.29	16	<1.0	7.9	77	22.5	2.1	1.6	0.66	−1.6	0.006	0.0010	34	<0.4
20	8.28	15	<1.0	7.8	79	23.2	2.1	1.6	0.66	−1.4	0.006	0.0009	35	<0.4

Samples 1–7 were collected in November 2006 and samples 8–20 in March 2007. Tributaries are indicated by the suffix 'T' in the sample label. Background water analysis was derived from averaged data from the nearby Wakatipu basin by Rosen & Jones (1998).

1985; Salzsauler et al. 2005; Langmuir et al. 2006; Paktunc et al. 2008; Haffert et al. 2010). Scorodite solubility is strongly controlled by pH, rising with rising pH to 10–100 mg/L As in circum-neutral waters (Fig. 9B) (Krause & Ettel 1988; Langmuir et al. 2006). Kankite, a more hydrous form of scorodite, probably has similar solubility to scorodite (Haffert et al. 2010). Scorodite is least soluble at a pH of c. 3–4.5 (<0.1 mg/L) and this solubility low coincides with the pH window of 2.5–3.5 found in the Bullendale mine waste (Fig. 9B, Fig. 10). If, however, the internal pH of the mine waste is modified by external neutralisation events, such as the addition of lime or flooding of the waste by carbonate-rich Skippers Creek water ('open system'), the pH of the waste will rise and scorodite solubility increases to hundreds of mg/L (Fig. 9B).

The increased solubility of ferric arsenate during such a flooding event is not likely to increase dissolved arsenic concentrations downstream, because of the increased dilution inherent in a flooding event. The addition of lime to the waste, however, would result in an increase in dissolved arsenic concentrations in Skippers Creek, especially during rain events. Increased mobility of arsenic from dissolved ferric arsenate would also result in a significant increase in the downstream arsenic flux due to the increased mobilisation of arsenic from the site, irrespective of downstream dilution.

The precipitation and stability of secondary Fe and As phases, in particular their cementing nature, also play a major role in the mine waste evolution. With increasing degree of cementation, the porosity decreases and the amount of percolating water is therefore limited. Most of the mine waste at the Phoenix battery is encapsulated and unavailable for weathering. Material underneath a well-cemented layer, such as the capping crust at the downstream waste pile, is also less exposed to weathering. Consequently, the secondary arsenic phases not only slow down arsenic mobilisation, but also reduce the surface area available for further weathering.

Impact of processing residues on water quality

The composition of Skippers Creek catchment water is strongly controlled by metamorphic calcite in the schist and localised ankerite associated with veins in altered rocks. Accordingly, catchment water is Ca-HCO$_3$ type, with an average pH of 8.3. The catchment water can be further subdivided into water that has only drained unaltered rock, and water that has interacted with altered rock. Skippers Creek, when approaching the site, drains bedrock affected by the mineralised Bullendale fault zone, but has not been affected by mining activity (sample 10$_T$, Fig. 1 and Table 1). This water composition is inferred to represent background water that has interacted with altered rocks. Analysis of
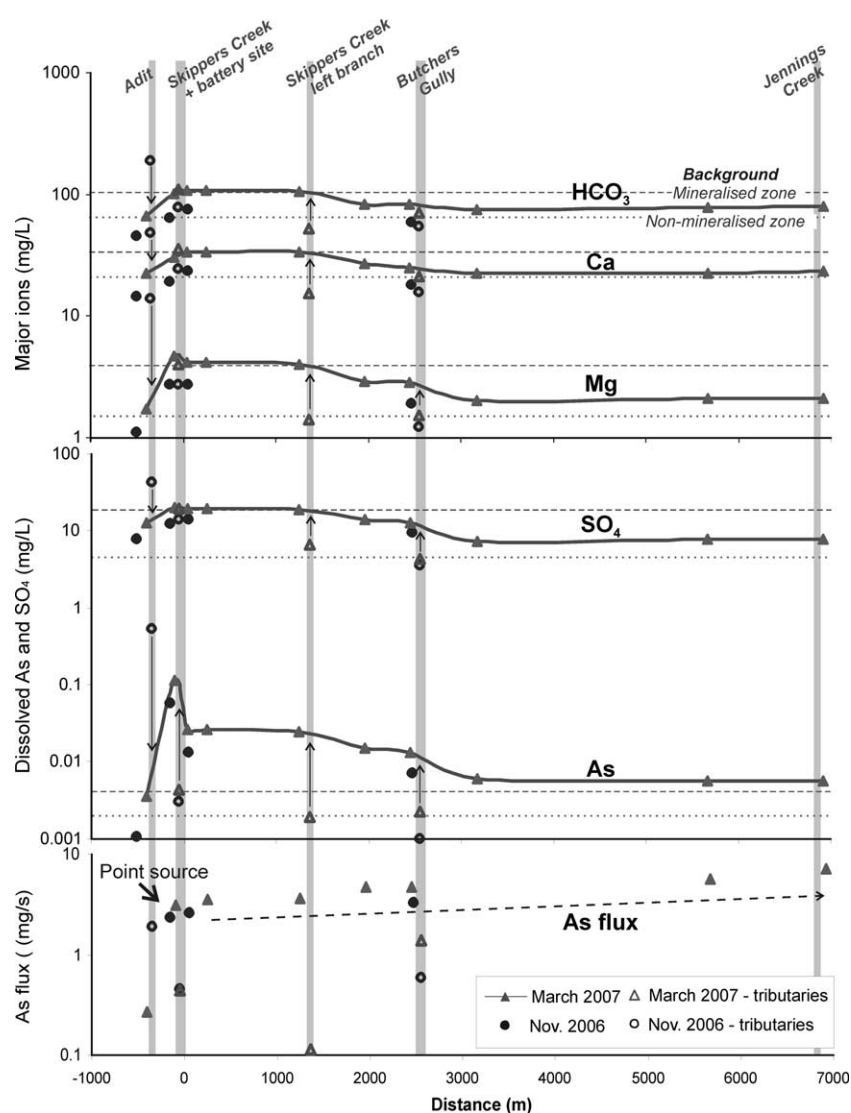
Fig. 7 Major ion, dissolved As and sulfate concentrations, and As flux with distance from the Phoenix battery.

downstream tributaries, such as the Skippers Creek left branch and the Butchers Gully, which do not drain mineralised rocks (e.g. sample 17_T, Fig. 1 and Table 1), represent regional background levels. Background waters were added to Fig. 7 to assist with the interpretation of the water composition data. Waters draining altered rock, and waters affected only by non-mineralised rock, are chemically distinctive (Fig. 7). Elevated dissolved magnesium, sulfate and arsenic concentrations are especially distinctive features of waters from mineralised rocks, because of the presence of ankerite, pyrite, and arsenopyrite. Arsenic is dissolved with sulfur from arsenopyrite in mineralised rock.

Adit discharge water upstream from the battery site has major ion concentrations typically half an order of magnitude higher than background water from mineralised rocks (Fig. 7). This water mixes with Murdochs Creek, which has at this point only drained a comparatively small part of the mineralised zone (Fig. 1). Coincidentally, the resultant

mixture has similar major ion content to the background water from mineralised rock, and the adit water does not cause an observable anomaly in Murdochs Creek when compared with local background levels. Arsenic, however, is two orders of magnitude higher in adit water compared with local background water (Fig. 6, Fig. 7), because of the enhanced amount of mineralised rock exposure in the underground shafts and adits that allow for increased arsenopyrite dissolution. Some of this arsenic is locally immobilised by ferrihydrite, which is present at the adit entrance.

There is no discernable signature of on-going arsenic-bearing seepage from the Phoenix battery site in the analysed waters from Murdochs Creek or Skippers Creek. This study was undertaken during a dry spell, and changes in water chemistry below the confluence of Murdochs Creek and Skippers Creek are attributed to the mixing of these two waters alone. However, some dissolved arsenic probably
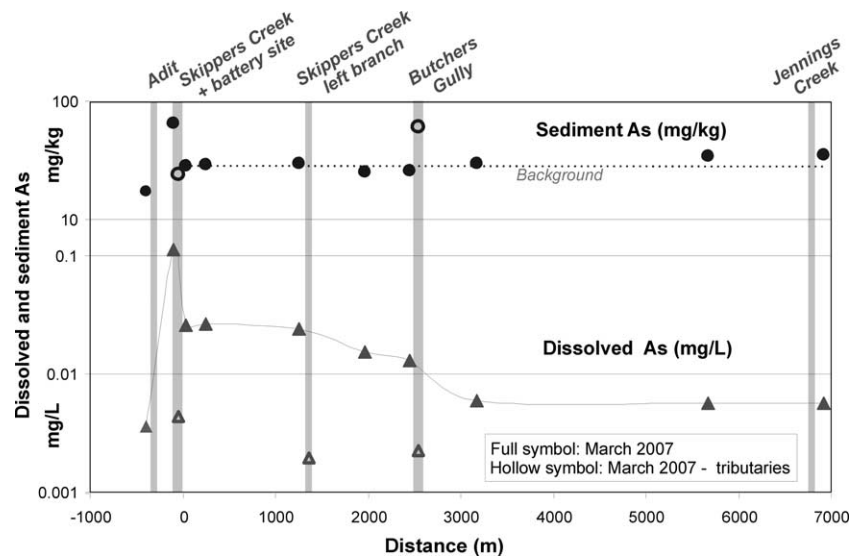
Fig. 8 Dissolved (triangle) and sediment (circle) As with distance from the Phoenix battery.

enters Skippers Creek with surface run-off during rain events, and the downstream arsenic profile could be significantly changed by this. For a holistic risk assessment of the site, the water quality within the streams at this site should be assessed under a range of rainfall events. This is of particular ecotoxicological significance, as many fauna can experience mortality or disrupted life cycles in response to short term (1–24 h) water quality decreases (US-EPA 1989).

Regional arsenic mobility

Arsenic attenuation

Arsenic is especially mobile in Skippers Creek catchment waters due to the high solubility of secondary arsenic minerals in alkaline waters (Fig. 9B). Furthermore, removal of arsenic into the sediment is rare, because common sorption sites for As, such as ferrihydrite and clay minerals, are absent from the Skippers Creek catchment due to the fast erosion rate of the mountainous region (see catchment description). The lack of interaction between sediment and dissolved arsenic is also reflected by the poor correlation between sediment arsenic and dissolved arsenic in Fig. 8. Instead, arsenic in sediment is mainly composed of eroded arsenopyrite from the various mineralised zones (Fig. 1) or boulders of mineralised rocks scattered throughout the catchment.

In the absence of removal of arsenic by secondary arsenic precipitation and/or adsorption, dilution of dissolved arsenic, which is generally less efficient, is the only attenuation process. Consequently, dissolved arsenic concentrations downstream from the adit remain elevated over the entire sampling distance. The anomaly not only exceeds natural background values, but also exceeds environmental guidelines. The adit water, presenting the highest dissolved arsenic concentrations encountered at this site, exceeds the Australian

and New Zealand Environmental and Conservation Council (ANZECC) guidelines for the 80% species survival (ANZECC 2000) by almost four times. Once diluted with Murdochs Creek, arsenic concentrations drop by an order of magnitude to below the 80% survival threshold.

Arsenic flux

In order to compare arsenic contribution from the Bullendale mine sites to background contribution from weathering of arsenopyrite-bearing bedrock, the arsenic flux was established where possible. From Fig. 7 it becomes apparent that the adit discharge water is a strong point source of arsenic, raising arsenic flux by over an order of magnitude. Downstream of the Bullendale mine, variations in arsenic flux are within the error of the relatively crude flow rate determination, but a slight overall increase can be recognised. Compared to arsenic input from the Bullendale adit, however, background contribution plays a comparatively small role because of limited chemical weathering of mineralised bedrock and sediment in the steep and intensely eroding terrain.

This observation is different from results obtained in other catchments in the South Island, where substantial natural input of arsenic has been identified (Hewlett et al. 2005; Haffert & Craw 2008b). Lower erosion rates and intense weathering of the rocks in these other catchments allow for increased background mobilisation of arsenic from arsenopyrite dissolution, resulting in high arsenic background fluxes compared to upstream point sources (Hewlett et al. 2005; Haffert & Craw 2008b). In these other catchments, sediments contain a significant proportion of adsorbed As and there is a strong correlation between sediment arsenic and dissolved arsenic, which was not observed in this study (Fig. 8).
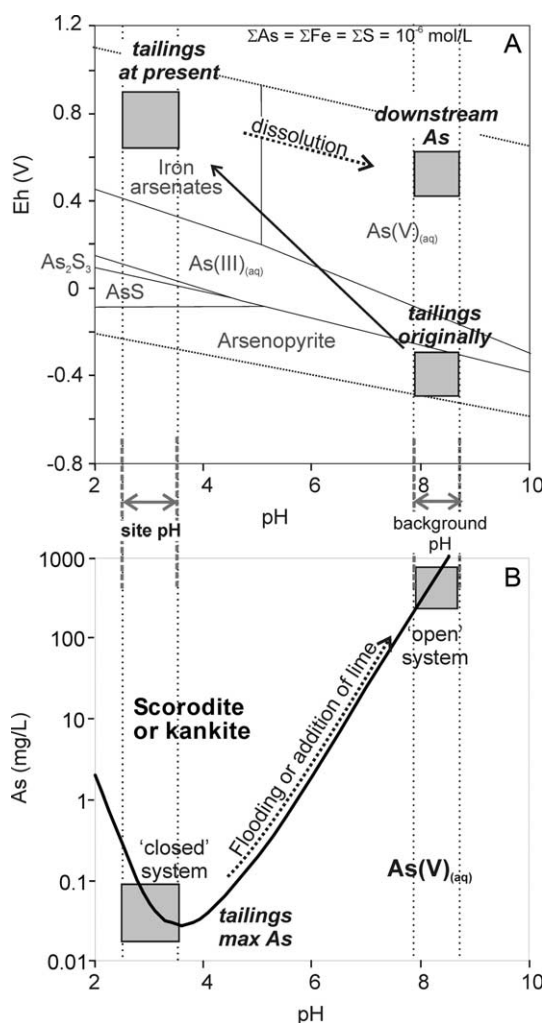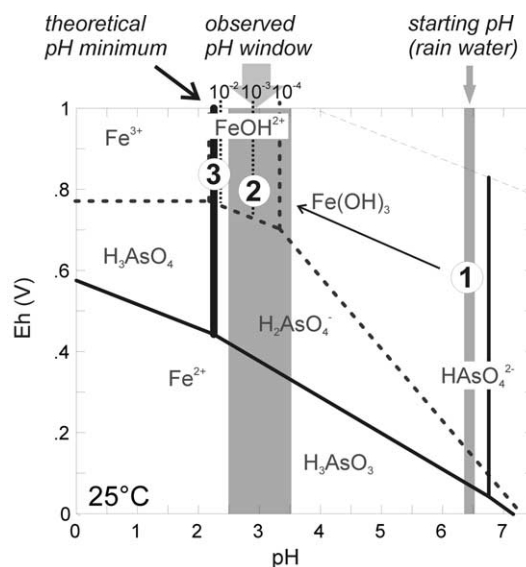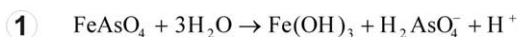
Fig. 9 (A) Eh-pH diagram with stability fields of As species, including scorodite and scorodite-like material, arsenopyrite, and dissolved species (Craw et al. 2003). The environmental conditions of the tailings originally and at present are indicated based on observations. (B) Solubility of scorodite after Krause & Ettel (1988). Without external modification ('closed system') the pH of the mine residues remain acidic and iron arsenate solubility is low. If neutralisation of mine residues occurs from external sources ('open system') iron arsenate solubility increases by several orders of magnitude.

Conclusions

Mine waste at the Phoenix battery contains very high arsenic concentrations (up to 40 wt%) and only minor Sb concentrations (up to 0.007 wt%). Roasting of the ore did not take place at this site and arsenic in processing residues was originally present only as arsenopyrite. Over the past 100 years, the primary arsenopyrite, which is unstable in the surficial environment, has oxidised and the waste is now dominated by secondary arsenic phases. From analytical data in conjunction with differences in morphology it
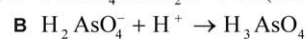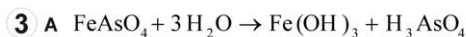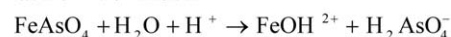

Fig. 10 Eh-pH diagram of dissolved As species (solid lines) and Fe species (broken line) at 10^{-4} mol/L. The observed pH window of mine residues is added. Reactions controlling pH are listed and the environment they occur in is indicated by circled numbers in the Eh-pH diagram.

becomes apparent that there is a mineralogical gradation between the ferrihydrite with varying amounts of adsorbed As, amorphous iron arsenates and crystalline kankite, scorodite, and zykaite. The pH of the mine waste is acidic, despite the absence of pyrite. This is due to reactions associated with iron arsenate dissolution, which maintain the pH between c. 2.5 and 3.5. At this pH, iron arsenate solubility is at a minimum and, at present, arsenic mobility from the waste pile is low. Mobility is further reduced by the limited exposure of arsenic-rich material due to the cementing nature of the secondary arsenic phases. In contrast to the battery site, the upstream adit is a constant source of arsenic to the environment. It creates a strong chemical anomaly, especially for arsenic, and because downstream attenuation takes place only via dilution, the anomaly persists for several kilometres downstream. Even when the effect of the anomaly has subsided, the arsenic flux of the river is still predominantly controlled by the adit input. This differs from catchments where intense weathering of mineralised bedrock provides a high background flux of arsenic and

point sources upstream only play a minor role in the downstream catchment.

References

American Public Health Association (APHA) 2005. 3125-B. Standard methods for the examination of water and waste-water. Washington DC, American Public Health Association.

Australian and New Zealand Environmental and Conservation Council (ANZECC) 2000. Australian and New Zealand guidelines for freshwater and marine water quality, paper no. 4. Canberra, Australian and New Zealand Environmental and Conservation Council.

Begbie MJ, Craw D 2006. Gold mineralisation in the Shotover–Macetown area, northwest Otago. In: Christie AB, Brathwaite RL eds. Geology and Exploration of New Zealand Mineral Deposits, Monograph 25. Melbourne, Australasian Institute of Mining and Metallurgy. Pp. 299–304.

Cooper AF, Barreiro BA, Kimbrough DL, Mattinson JM 1987. Lamprophyre dike intrusion and the age of the Alpine Fault, New Zealand. Geology 15: 941–944.

Craw D 1989. Shallow-level, late-stage gold mineralisation in Sawyers Creek, Shotover valley, northwest Otago, New Zealand. New Zealand Journal of Geology and Geophysics 32: 385–393.

Craw D 2001. Tectonic controls on gold deposits and their environmental impact, New Zealand. Journal of Geochemical Exploration 73: 43–56.

Craw D 2002. Geochemistry of late metamorphic hydrothermal alteration and graphitisation of host rock, Macraes gold mine, Otago Schist, New Zealand. Chemical Geology 191: 127–275.

Craw D, Norris RJ 1991. Metamorphic Au-W veins and regional tectonics: mineralisation throughout the uplift history of the Haast Schist, New Zealand. New Zealand Journal of Geology and Geophysics 34: 373–383.

Craw D, Chappel D, Reay A, Walls D 2000. Mobilisation and attenuation of arsenic around gold mines, east Otago, New Zealand. New Zealand Journal of Geology and Geophysics 43: 373–383.

Craw D, Pacheco L 2002. Mobilisation and bioavailability of arsenic around mesothermal gold deposits in a semiarid environment, Otago, New Zealand. The Scientific World Journal 2: 308–319.

Craw D, Falconer D, Youngson JH 2003. Environmental arseno-pyrite stability and dissolution: theory, experiment, and field observations. Chemical Geology 199: 71–82.

Craw D, Wilson N, Ashley PM 2004. Geochemical controls on the environmental mobility of Sb and As in mesothermal antimony and gold deposits. Transactions of the Institute of Mining and Metallurgy 113: B3–B10.

Craw D, Begbie M, MacKenzie D 2006. Structural controls on tertiary orogenic gold mineralization during initiation of a mountain belt, New Zealand. Mineralium Deposita 41: 645–659.

Craw D, Rufaut CG, Hammitt S, Clearwater S, Smith CM 2007. Geological controls on natural ecosystem recovery on mine waste in southern New Zealand. Environmental Geology 51: 1389–1400.

Dove PM, Rimstidt JD 1985. The solubility and stability of scorodite, $FeAsO_4 \cdot 2H_2O$. American Mineralogist 70: 838–844.

Foy CD, Chaney RL, White MC 1978. The physiology of metal toxicity in plants. Annual Review of Plant Physiolology 29: 511–566.

Haffert L, Craw D 2008a. Mineralogical controls on environmental mobility of As (III) and (V) from historic mine processing residues, New Zealand. Applied Geochemistry 23: 1467–1483.

Haffert L, Craw D 2008b. Processes of attenuation of dissolved arsenic downstream from historic gold mine sites, New Zealand. Science of the Total Environment 405: 286–300.

Haffert L, Craw D, Pope J 2010. Climatic and compositional controls on secondary arsenic mineral formation in high-arsenic mine wastes, South Island, New Zealand. New Zealand Journal of Geology and Geophysics 53: 91–101.

Hamel J 2001. The archaeology of Otago. Wellington, Department of Conservation.

Hewlett L, Craw D, Black A 2005. Comparison of trace element contents of discharges from adjacent coal and gold mines, Reefton, New Zealand. Marine and Freshwater Research 56: 983–995.

Hutchison I, Ellison RD 1992. Mine waste management, California Mining Association. Chelsea MI, Lewis Publishers.

Krause E, Ettel VA 1988. Solubility and stability of scorodite, $FeAsO_4 \cdot 2H_2O$: new data and further discussion. American Mineralogist 73: 850–854.

Langmuir D, Mahoney J, Rowson J 2006. Solubility products of amorphous ferric arsenate and crystalline scorodite (FeAsO4·2H2O) and their application to arsenic behaviour in buried mine tailings. Geochimica et Cosmochimica Acta 70: 2942–2956.

MacKenzie DJ, Craw D, Begbie M 2007. Mineralogy, geochemistry, and structural controls of a disseminated gold-bearing alteration halo around the schist-hosted Bullendale orogenic gold deposit, New Zealand. Journal of Geochemical Exploration 93: 160–176.

MacKinnon TC 1983. Origin of the Torlesse terrane and coeval rocks, South Island, New Zealand. Geological Society of America Bulletin 94: 967–985.

Mortimer N 1993. Geological map of the Otago Schist and adjacent rocks, 1: 500000, Institute of Geological & Nuclear Sciences Map 7. Wellington, New Zealand, Institute of Geological & Nuclear Sciences.

Mortimer N 2000. Metamorphic discontinuities in orogenic belts: example of the garnet-biotite-albite zone in the Otago Schist, New Zealand. International Journal of Earth Sciences 89: 295–306.

Paktunc D, Dutrizac J, Gertsman V 2008. Synthesis and phase transformations involving scorodite, ferric arsenate and arsenical ferrihydrite: implications for arsenic mobility. Geochimica et Cosmochimica Acta 72: 2649–2672.

Petchey P 2002. Archaeological survey of the Arrow River and Macetown, Otago. Wellington, New Zealand, Department of Conservation.

Petchey PG 2006. Gold and electricity. Archaeological survey of Bullendale, Otago. Wellington, Science and Technical Publishing, Department of Conservation.

Roddick-Lanzilotta AJ, McQuillan AJ, Craw D 2002. Infrared spectroscopic characterisation of arsenate (V) ion adsorption from mine waters, Macraes mine, New Zealand. Applied Geochemistry 17: 445–454.

Rosen M, Jones S 1998. Controls on the chemical composition of groundwater from alluvial aquifers in the Wanaka and Wakatipu basis, Central Otago, New Zealand. Hydrogeology Journal 6: 264–284.

Salzsauler KA, Sidenko NV, Sheriff BL 2005. Arsenic mobility in alteration products of sulfide-rich, arsenopyrite-bearing mine wastes, Snow Lake, Manitoba, Canada. Applied Geochemistry 20: 2303–2314.

Smedley PL, Kinniburgh DG 2002. A review of the source, behaviour and distribution of arsenic in natural waters. Applied Geochemistry 17: 517–568.

Sobek A, Schuller WA, Freeman JR, Smith RM 1978. Field and laboratory methods applicable to oberburden and minesoils. Cincinnati, Ohio, US Environmental Protection Agency. EPA-600/2-78-054.

United States Environmental Protection Agency (US-EPA) 1989. Exposure factors handbook. Washington DC, Office of Health and Environmental Assessment. EPA/600/8-89/043.

United States Environmental Protection Agency (US-EPA) 1994. Methods for the determination of metals in environmental samples, Supplement 1. EPA 600-R94-111.

Williams GJ 1974. Economic geology of New Zealand. Australasian Institute of Mining and Metallurgy Monograph 4. Melbourne, Australasian Institute of Mining and Metallurgy.